HHS Public Access

Author manuscript

J Phys Chem B. Author manuscript; available in PMC 2016 February 24.

Published in final edited form as:

J Phys Chem B. 2015 September 3; 119(35): 11581–11589. doi:10.1021/acs.jpcb.5b06171.

^{15}N and ^{1}H Solid-State NMR Investigation of a Canonical Low-Barrier Hydrogen-Bond Compound: 1,8-bis(dimethylamino) naphthalene

Paul B. White and **Mei Hong***

Department of Chemistry, Massachusetts Institute of Technology, 170 Albany Street, Cambridge, MA 02139

Abstract

Strong or low-barrier hydrogen bonds have been often proposed in proteins to explain enzyme catalysis and proton transfer reactions. So far ^{1}H chemical shifts and scalar couplings have been used as the main NMR spectroscopic signatures for strong H-bonds. In this work, we report simultaneous measurements of ^{15}N and ^{1}H chemical shifts and N-H bond lengths by solid-state NMR in ^{15}N-labeled 1,8-bis(dimethylamino) naphthalene (DMAN), which contains a well known strong NHN H-bond. We complexed DMAN with three different counter anions to examine the effects of the chemical environment on the H-bond lengths and chemical shifts. All three DMAN compounds exhibit significantly elongated N-H distances compared to the covalent bond length, and the $^{1}H^{N}$ chemical shifts are larger than ~17 ppm, consistent with strong NHN H-bonds in the DMAN cation. However, the ^{15}N and ^{1}H chemical shifts and the precise N-H distances differ among the three compounds, and the ^{15}N chemical shifts show opposite dependences on the proton localization from the general trend in organic compounds, indicating the significant effects of the counter anions on the electronic structure of the H-bond. These data provide useful NMR benchmarks for strong H-bonds, and caution against the sole reliance on chemical shifts for identifying strong H-bonds in proteins, since neighboring sidechains can exert similar influences on chemical shifts as the bulky organic anions in DMAN. Instead, N-H bond lengths should be measured, in conjunction with chemical shifts, as a more fundamental parameter of H-bond strength.

Graphical abstract

Corresponding author: Mei Hong, meihong@mit.edu.

Supporting Information Available: Full author lists for references with more than ten authors. This material is available free of charge via the Internet at http://pubs.acs.org.

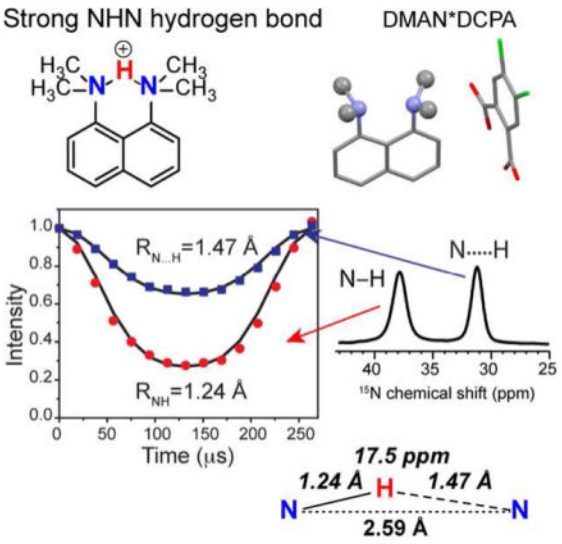

Keywords

Low-barrier hydrogen bonds; N-H bond lengths; influenza M2; DIPSHIFT; strong hydrogen bonds

Introduction

Hydrogen bonding is ubiquitous in biological systems, and strong hydrogen bonds (H-bonds) have been proposed to play important roles in enzyme catalysis [1–5] and proton transfer reactions in photoreceptors [6–9] and ion channels [10–11]. However, the nature and function of strong H-bonds have been the subject of significant debate in the literature. Early NMR spectroscopic studies of the catalytic triad of α-chymotrypsin reported an unusually large ^{1}H chemical shift of ~18 ppm for the proton bound to Nδ1 of His57 [12]. Combined with subsequent findings of low ^{1}H/^{2}H fractionation factors and large chemical shift perturbation, these data supported the existence of strong H-bonds in this and other enzymes [13–15].

The fundamental criterion for classifying H-bond strengths is the potential energy curve (Scheme 1). Strong H-bonds are characterized by the fact that the ground vibrational mode for proton motion lies either near or above the energy barrier for proton transfer [12, 16–17]. Two types of strong H-bonds are especially noteworthy: single-well H-bonds, which have no barrier for proton transfer, and low-barrier H-bonds (LBHB), which has a double-well energy minimum (Scheme 1e, f). In both these strong H-bonds, the probability density function for proton position has a single maximum at the center of the two heteroatoms. A rigorous identification of the nature of H-bonds thus requires a study of the system's electronic and energetic states, which have been conducted largely with computational methods [18–20].

Since potential energies of H-bonds are difficult to measure experimentally, distances have been used as alternative criteria for classifying H-bonds. For NHN compounds, these are the distance between the donor and acceptor nitrogens, R_{NN}, and the distances of the proton

(H^N) from the donor (R_{NH}) and acceptor (R_{N---H}). At one end of the hydrogen bonding spectrum are weak or regular H-bonds (Scheme 1a), in which the ground vibrational energy is much lower than the proton-transfer barrier, thus the probability density function for the proton has two maxima, centered near each heteroatom. Weak NHN H-bonds exhibit a much shorter R_{NH} than R_{N---H}, an R_{NN} distance longer than 3.0 Å, and are primarily electrostatic in nature [21–22]. As the H-bonding strength increases, the H^N moves progressively towards the center of the two nitrogens, and R_{NN} decreases, making the bond more covalent than electrostatic. Strong NHN H-bonds (Scheme 1c, e, f) have $R_{NN} \leq 2.65$ Å. The degree of covalency of the H-bonds is manifested by the chemical shift of the intervening proton and the two-bond J-couplings between the nitrogens, $^{2h}J_{NN}$ [23–27]: both the ^{1}H chemical shift and $^{2h}J_{NN}$ increase as the proton becomes more delocalized and the H-bond strength increases. For LBHBs (Scheme 1e), the shared proton between the donor and acceptor is expected to have a chemical shift above ~17 ppm [28–29].

We became interested in better understanding H-bonds in biological systems through our studies of the influenza A M2 protein [30]. M2 forms a tetrameric proton channel in the virus envelope that is responsible for the acidification of the virion and the subsequent virus uncoating. The proton-selective residue in M2 is a single histidine, His37, in the transmembrane domain [31], which contains both a H-bond donor (N-H) and acceptor (N:) in the imidazole ring. Several mechanisms of proton conduction have been proposed. In the shuttle model, the His37 imidazole alternately protonates and deprotonates by proton transfer with water molecules [32]. To generate the initial state for the next proton relay, the imidazole was thought to undergo ring flips and tautomerization, both of which have been observed experimentally [33–34]. The H-bonds in this shuttle model are weak NHO H-bonds between histidine and water. A high-resolution crystal structure reported tightly bound water molecules in the vicinity of the H37 tetrad [35], and low-temperature imidazole H^N chemical shifts measured by NMR under conditions where proton transfer is frozen are less than 15 ppm, supporting weak to moderate H-bonds. Moreover, at high temperature when proton exchange is active, the imidazole H^N chemical shifts change to the water ^{1}H chemical shift value of ~4.9 ppm, indicating that the H-bonding partner of His37 sidechain is water [36]. These lines of evidence support the weak water-histidine H-bonded shuttle mechanism. In comparison, an alternative proton-conduction model posits that a neutral imidazole ring of one polypeptide chain forms a strong or low-barrier H-bond with a cationic imidazolium of a neighboring chain at mildly acidic pH, prior to channel activation at lower pH [10–11]. This model was proposed to explain the observations that the first two pK_a's of the His37 tetrad are significantly elevated (8.2) compared to the typical pK_a of histidines in solution and moreover are unresolved [10], suggesting that the M2 channel is able to store +2 charges before it becomes conductive. It is thought that a strong or low-barrier imidazole-imidazolium NHN H-bond can provide the mechanism for this charge stabilization. An implication of this LBHB model is that the tetramer consists of two structurally distinct units, or a dimer of dimers. Partial evidence for dimer formation was reported as doubled NMR chemical shifts for many residues in the protein [37–39]; however, this chemical shift doubling was observed at high pH where all histidines are neutral, thus violating the requirement of an imidazole-imidazolium pair in the LBHB model.

These studies of H-bonding in M2 and other complex biological systems inspired us to obtain better and clearer solid-state NMR (SSNMR) signatures of strong H-bonds, to correlate multiple signatures, and to delineate the environmental factors that may affect the H-bond strengths or their manifestations. So far few studies have correlated the readily measureable ^{1}H and ^{15}N chemical shifts with the less easily measured but more definitive parameter of R_{NH} distances. Given vibrational averaging effects and the low electron density of protons, N-H bond lengths obtained from X-ray crystallography are often imprecise and shorter than those measured by neutron diffraction and SSNMR. Thus, it is important to directly measure, in known strong H-bonds, R_{NH} distances by NMR and correlate them with ^{15}N and ^{1}H chemical shifts. In this paper, we report a systematic study of these three NMR observables for the 1,8-bis(dimethylamino)-naphthalene (DMAN) family of strong H-bond compounds. X-ray and neutron diffraction of DMAN salts showed R_{NN} distances of 2.55 Å – 2.63 Å [22, 40–43]. For a small number of these compounds, $R_{N\text{-}H}$ and $R_{N\text{---}H}$ distances have been reported by X-ray crystallography and found to range from equivalent (1.31 Å) to off-center. ^{1}H NMR chemical shifts of >18 ppm have been reported for DMAN salts containing small inorganic counterions [28, 43], but DMAN cations that are complexed with bulky organic anions, which better mimic protein sidechains, are less studied. We have thus chosen several DMAN compounds with organic counter anions, synthesized them with ^{15}N and ^{13}C labeling, and measured N-H bond lengths, ^{15}N and ^{1}H chemical shifts. The results should provide useful NMR fingerprints of strong H-bonds in biological macromolecules.

Experimental

Synthesis of ^{15}N, ^{13}C-labeled DMAN

DMAN was synthesized using modified literature procedures outlined in Scheme 2 [44–47]. Naphthalene (783 mg, 6.12 mmol), $NH_4\,^{15}NO_3$ (1 g, 12.3 mmol, 2.01 eq) and chloroform (6 mL) were added to a 50 mL round bottom flask and the mixture stirred. An addition funnel was added to the top of the flask and the whole system placed under N_2 gas. Trifluoroacetic anhydride (5 mL, 35.4 mmol, 5.8 eq) was added to the addition funnel and introduced to the reaction flask via slow drip over 1.5 hours. The solution became homogeneous and changed from colorless to rose to yellow during the addition. The reaction was stirred overnight under N_2. The resulting heterogeneous reaction mixture was then put on ice and 10 mL of H_2O was slowly added to the flask by addition funnel to quench excess TFAA. The contents were poured into a separatory funnel containing 60 mL H_2O and 20 mL $CHCl_3$. The organic layer was extracted three more times with 20 mL $CHCl_3$ and the combined organic fractions were dried over $MgSO_4$, filtered and the solvent removed on a rotary evaporator to yield an orange-yellow crude mixture consisting of a 3 : 1 mixture of $^{15}N_2$-1,8-dinitronaphthalene and $^{15}N_2$-1,5-dinitronaphthalene (1.25 g, 93%). The 1,8 isomer was purified first with a basic Al_2O_3 column and eluted with benzene (1,8 isomer: Rf = 0.4; 1,5 isomer: Rf = 0.76). The 1,8-rich fractions were collected and recrystallized three times with EtOAc. The supernatant of each crystallization was collected and the solvent removed under reduced pressure. The resulting solid was again recrystallized with EtOAc. The recrystallization process was repeated one more time to give a total of 608 mg (65% recovery, 49% overall yield) $^{15}N_2$-1,8-dinitronaphthalene as yellow plates. ^{1}H NMR (400 MHz, $CDCl_3$): δ 7.75

(t, $^{3}J_{HH}$ = 7.9 Hz, 2H), 8.24 (d, $^{3}J_{HH}$ = 8.3 Hz, 2H), 8.30 (dd, $^{3}J_{HH}$ = 7.6 Hz, $^{3}J_{NH}$ = 2 Hz, 2H).

$^{15}N_2$-labeled 1,8-dinitronaphthalene (604 mg, 2.74 mmol), $FeCl_3$ hexahydrate (22 mg, 3 mol %) and 45 mg Nuchar SA activated carbon were combined in a 25 mL round bottom flask equipped with a stir bar and reflux condenser. MeOH (6 mL) and 50–60% N_2H_4 (464 μL, 5.45 eq) were added, the reaction stirred and heated to 65 °C. After 5.5 hrs an aliquot was removed and the reaction progress was checked by ^{1}H NMR. There was 7% remaining starting material so two drops of hydrazine were added and stirred for another hour, after which no more starting material was observed. The reaction was cooled to room temperature, filtered over Celite and the filter cake-washed with MeOH. The filtrate was removed under reduced pressure to yield a crude oil (430 mg, 98%), which was the pure $^{15}N_2$-1,8-diaminonaphthalene compound as verified by NMR. $^{15}N_2$-1,8-diaminonaphthalene was used without purification for the next step. ^{1}H NMR (400 MHz, $CDCl_3$): δ 4.62 (bs, 4H, $^{15}NH_2$), 6.60 (d, $^{3}J_{HH}$ = 7 Hz, 2H), 7.15–7.22 (m, 4H).

$^{15}N_2$-1,8-diaminonaphthalene (430 mg, 2.68 mmol) was added to a 10 mL round bottom flask equipped with a stir bar and placed under N_2 gas. Anhydrous DMSO (4 mL) was quickly added, the contents stirred and then KOH (775 mg, 5.15 eq) was quickly added. The flask was placed in a room-temperature water bath, to which ^{13}CHI (950 μL, 5.6 eq) was slowly added and stirred for 2.25 hrs. The temperature was then raised to 100 °C over 1 hr, at which point KOH (320 mg, 2.1 eq) was added. The reaction was stirred at 100 °C for another 40 minutes and then cooled to 50 °C. The reaction contents were quickly poured into a separatory funnel containing 150 mL 2 M NaOH and 50 mL Et_2O. The organic layer was washed 3 × 50 mL 2 M NaOH and then collected. The combined aqueous layers were extracted with 2 × 50 mL Et_2O. The combined organic layers were dried with $MgSO_4$, filtered and the solvent removed under reduced pressure, resulting in a red oil (532 mg, 2.42 mmol, 90%) that crystallized into needles upon refrigerating and was pure by ^{1}H NMR. δ 2.83 (dd, $^{1}J_{CH}$ = 138.7 Hz, $^{2}J_{NH}$ = 4.1 Hz, 12H), 6.96 (broad d, $^{3}J_{HH}$ = 7.4 Hz, 2H), 7.33 (t, $^{3}J_{HH}$ = 7.6 Hz, 2H), 7.38 (d, $^{3}J_{HH}$ = 7.7 Hz, 2H).

The ^{15}N, ^{13}C-labeled $DMANH^+$ salts were recrystallized with three counterions: perchlorate ($HClO_4$), 4,5-dichlorophthalic acid (DCPA), and furan-3,4-dicarboxylic acid (FDCA). DMAN*$HClO_4$ was formed by dissolving DMAN in diethyl ether, stirring the solution and adding concentrated aq. $HClO_4$ dropwise. DMAN*$HClO_4$ precipitated as a brown material, and the addition of $HClO_4$ was ceased when no more precipitate formed. The stirring was then stopped, the supernatant pipetted out, the precipitate washed three times with diethyl ether and then dried under vacuum. The resulting goo was recrystallized twice from a minimal amount of boiling acetonitrile. DMAN*DCPA and DMAN*FDCA were formed by adding DMAN and the respective acid as solids into a 1.5 mL HPLC vial, dissolving them in a minimal amount of hot acetonitrile and then letting the solution cool. Afterwards, the DMAN*DCPA and DMAN*FDCA solutions were allowed to evaporate slowly at room temperature. The resulting crystals were recrystallized once more, washed with a very small amount of cold acetonitrile, and dried. The structures of DMAN*$HClO_4$ and DMAN*FDCA were solved using X-ray diffraction, since no structure existed for DMAN*$HClO_4$ and, despite multiple attempts, the exact unit cell obtained by Wozniak for DMAN*FDCA could

not be reproduced.[42] Instead, a unique unit cell with the same molecular composition (DMAN + FDCA + water) was obtained. The unit cell of DMAN*DCPA matched the literature unit cell and no further X-ray analysis was performed.

Solid-state NMR spectroscopy

All experiments were conducted using Bruker 400 and 600 MHz solid-state NMR spectrometers equipped with 4 mm or 3.2 mm magic-angle-spinning (MAS) probes. Typical radiofrequency (rf) field strengths were 40–50 kHz for ^{15}N and 80 – 100 kHz for ^{1}H. The experiments were conducted at both ambient temperature and 95 K to investigate the degree of proton dynamics at ambient temperature. ^{15}N cross-polarization (CP) spectra were measured under an MAS frequency of 7.58 kHz, while ^{1}H spectra were measured under 15 kHz MAS. ^{15}N chemical shifts were externally referenced to the N-acetyl-valine ^{15}N chemical shift of 122.0 ppm on the liquid ammonium scale. ^{1}H chemical shifts were referenced to the published values of the tripeptide formyl-MLF-OH [48]. N-H bond lengths were measured using the dipolar-doubled 2D ^{15}N-^{1}H dipolar chemical-shift (DIPSHIFT) correlation experiment [49] under 3.79 kHz MAS. ^{1}H homonuclear decoupling was conducted using the FSLG sequence [50], which has a theoretical scaling factor of 0.577. The experimental scaling factor was measured using formyl-MLF-OH [51–52] and found to be 0.577 at ambient temperature and 0.610 at 95 K. 2D ^{15}N-^{1}H HETCOR spectra were measured under 7.58 kHz MAS. Lee-Goldburg (LG) CP [53–54] with a 1 ms contact time and a 50 kHz effective spin-lock field was used to transfer the ^{1}H polarization to ^{15}N without ^{1}H spin diffusion. ^{1}H homonuclear decoupling during the t_1 evolution period was carried out using the FSLG sequence with a transverse field strength of 80 kHz.

Results

X-ray diffraction data of selected DMAN compounds

We chose three compounds from the many known DMAN salts using two criteria [40, 42, 55–57]. First, each recrystallization should give a single crystalline form, since bulk separation of polymorphic crystals is often incomplete, which would complicate spectral interpretation. Second, DMAN salts with a highly delocalized proton as well as more localized protons are needed to compare the chemical shifts and bond lengths for different strengths of H-bonds. Based on the literature, we chose DMAN*DCPA and DMAN*FDCA as examples of salts with bulky organic counter anions (Fig. 1) [42] that contain partly localized H^N protons and DMAN*$HClO_4$ as a potential model system with a delocalized H^N.

We first verified the structures of the recrystallized DMAN salts by X-ray diffraction (Fig. 1). DMAN*$HClO_4$ has not been previously characterized by X-ray diffraction, thus a full atomic structure was determined. The unit cell for DMAN*DCPA matched the literature result while the unit cell of DMAN*FDCA differed significantly from the literature [42] (Table 1). Upon obtaining a full data set, we found that the FDCA in our crystal has a different spatial arrangement with respect to the DMAN cation. In addition, there is one equivalent of water in the DMAN*FDCA unit cell, which is absent in the other two salts, but the water molecule has a different position in our crystal from that of the literature.

Comparison of the three DMAN crystal structures reveals small but important differences. First, despite the common cation, the R_{NN} distance differs among the three compounds. The distance is the shortest for DMAN*$HClO_4$ (2.55 Å) and increases to 2.59 Å for DMAN*DCPA and 2.62 Å for DMAN*FDCA. Second, the inorganic perchlorate anion rests proximally above the NHN H-bond, roughly equidistant to the two dimethylamino groups, whereas the organic DCPA and FDCA anions lie on one side of the NHN H-bond. The nearest heavy-atom distance between the nitrogen donor/acceptors and the counter anion is 3.30 Å for DMAN*$HClO_4$, 3.85 Å for DMAN*DCPA, and 3.64 Å for DMAN*FDCA. The proximity and orientation of the anion to the NHN H-bond and the differences in R_{NN} may affect the localization of the proton by changing the chemical environment at the nitrogen donors and acceptors.

^{15}N chemical shifts and N-H distances of DMAN salts

Fig. 2 shows the ^{15}N CP-MAS spectra of the three DMAN compounds at 283 K and 95 K. Consistent with the crystal structure, the compound with the shortest R_{NN} distance and the highest unit cell symmetry, DMAN*$HClO_4$, exhibits a single ^{15}N peak at 35.4 ppm. In comparison, DMAN*DCPA and DMAN*FDCA display two ^{15}N chemical shifts: 37.8 ppm and 31.2 ppm for the DCPA salt and 39.5 ppm and 29.3 ppm for the FDCA salt, suggesting that the proton is located asymmetrically between the two nitrogens. DMAN*DCPA has a smaller ^{15}N chemical shift difference (6.6 ppm) than DMAN*FDCA (10.2 ppm), but the average of the two ^{15}N chemical shifts, 34.4 ppm, is close to the single ^{15}N chemical shift of DMAN*$HClO_4$.

In general, ^{15}N chemical shifts of organic compounds follow the trend that larger (downfield) shifts correspond to more deprotonated nitrogens with longer R_{NH} bond lengths, while smaller (upfield) chemical shifts indicate more protonated nitrogens with shorter R_{NH} bond lengths. Interestingly, direct measurement of the N-H distance in the three DMAN compounds shows deviations from this rule. We used the dipolar-doubled DIPSHIFT experiment to measure the ^{15}N-^{1}H dipolar coupling and R_{NH} distances (Fig. 3). Motion in these rigid organic crystals is negligible, thus the measured coupling constant directly indicates the internuclear distance. At ambient temperature, the single ^{15}N peak of the perchlorate compound exhibits a ^{15}N-^{1}H dipolar coupling of 5.39 kHz, which translates to an R_{NH} of 1.32 Å. This distance is in good agreement with the R_{NH} of 1.31 Å in the crystal structure of DMAN salts that contain an equally shared proton, such as DMAN*HBr [56] and DMAN*tetrazole [40]. In DMAN*DCPA, the downfield peak has a 6.50 kHz coupling, corresponding to an R_{NH} of 1.24 Å, while the upfield ^{15}N peak has a longer R_{NH} of 1.47 Å. For DMAN*FDCA, the downfield ^{15}N peak has an R_{NH} distance of 1.23 Å while the upfield ^{15}N peak has an R_{NH} of 1.49 Å. Thus, for the DCPA and FDCA salts, the more deshielded (or downfield) ^{15}N resonance has a *stronger* ^{15}N-^{1}H dipolar coupling or a *shorter* R_{NH} bond length than the upfield ^{15}N peak, opposite the general trend, suggesting that the two nitrogens' spectroscopic signatures are significantly perturbed by the counter anions.

We repeated the ^{15}N CP-MAS and N-H DIPSHIFT experiments at 95 K to determine if there is noticeable proton dynamics at ambient temperature and if the H^N proton becomes

more localized to one of the two nitrogens at low temperature. The ^{15}N chemical shift showed negligible changes with temperature, but the linewidth broadened significantly for DMAN*$HClO_4$, from 55 Hz at ambient temperature to 109 Hz at 95 K. In comparison, the DMAN*DCPA and DMAN*FDCA ^{15}N peaks show only minor line broadening of ~10 Hz. The ^{15}N-^{1}H dipolar couplings remain unchanged within experimental uncertainty from 293 K to 95 K, indicating that the H^N position is insensitive to temperature in this range.

$^{1}H^{N}$ chemical shifts of DMAN salts

We next measured the acidic proton's chemical shift to correlate with the ^{15}N chemical shift and R_{NH} bond lengths. The chemical shift differences between the H^N and aliphatic protons are sufficiently large that 1D ^{1}H MAS spectra are already effective in resolving them (Fig. 4). At 600 MHz under 15 kHz MAS, the 1D ^{1}H spectra show sufficient resolution at both 283 K and 95 K. For DMAN*$HClO_4$, the NHN^+ proton resonates at 18.9 ppm while the methyl protons resonate at 3.50 ppm and 1.70 ppm, in good agreement with literature values [43]. In addition, two resonances at 6.87 ppm and 5.48 ppm were observed and assigned to aromatic protons.

The ^{1}H spectrum of DMAN*DCPA shows more resolved peaks. Two large ^{1}H chemical shifts at 20.76 ppm and 17.52 ppm are detected and likely correspond to the OHO^- proton of the DCPA anion and the NHN^+ proton of the DMAN cation, respectively. The 8.59 ppm and 6.52 ppm peaks can be assigned to the naphthalene ring protons, while the 3.70 ppm and 1.41 ppm peaks are assigned to the *N*-methyl groups. DMAN*FDCA exhibited a single downfield ^{1}H peak at 17.26 ppm, despite having a similar OHO^- proton as in DMAN*DCPA. We attribute this to coincidental overlap of the NHN^+ and OHO^- chemical shifts, which is consistent with the high intensity of this peak compared to the aromatic and aliphatic signals. Similar to DMAN*DCPA, the aromatic ^{1}H resonances are well resolved at 8.25 ppm and the methyl ^{1}H signals span from 3.63 ppm to −0.47 ppm. The −0.47 ppm resonance likely results from the methyl group that is flanked by the π-cloud of the FDCA anion and the naphthalene ring of a neighboring $DMANH^+$ cation in the crystal lattice, which causes additional shielding from the aromatic electrons.

For DMAN*DCPA, the 1D ^{1}H MAS spectrum alone cannot unambiguously determine which of the two downfield signals belongs to the NHN^+ H-bond. Thus, we measured 2D ^{15}N-^{1}H HETCOR spectra to make a definitive assignment. Fig. 5 shows two ^{1}H-^{15}N cross peaks at (17.4 ppm, 37.8 ppm) and (17.4 ppm, 31.2 ppm), thus confirming the assignment of the NHN^+ proton to 17.4 ppm. The OHO^- proton then resonates at 20.76 ppm, consistent with the fact that it lies in a very short and strong H-bond. The 2D HETCOR spectra of the other two DMAN compounds (not shown) also confirmed the ^{1}H chemical shift assignment in the 1D ^{1}H spectra.

Discussion

While hydrogen bonding has undisputed importance in biological and synthetic compounds, rigorous studies of the NMR signatures of hydrogen bonding in the solid state are relatively scarce. McDermott and coworkers investigated NHN H-bonds in imidazole - imidazolium complexes with different counterions by measuring temperature-dependent ^{15}N chemical

shifts and correlating these with crystallographically determined R_{NN} distances [58]. The R_{NN} were 2.65 – 2.68 Å, which are slightly longer than the cutoff for strong H-bonds. Their NMR data revealed the presence of fast proton exchange in some of the salts from 200 to 280 K, and the population of the two protonation states is strongly dependent on temperature and counter anions. At 210 K, these workers measured an R_{NH} distance of 1.10 Å, which is close to the covalent bond length of R_{NH} = 1.05 Å in imidazole [22]. The temperature-dependent ^{15}N chemical shifts, near-covalent R_{NH} bond lengths, and the modest R_{NN} distances, together indicate that the imidazole – imidazolium complexes contain weak to moderate H-bonds.

The *intramolecular* strong H-bonds formed by DMAN differ qualitatively from the intermolecular weak H-bonds in imidazoles. Fig. 6 summarizes the measured chemical shifts and R_{NH} distances in our DMAN compounds. All three compounds show $^{1}H^{N}$ chemical shifts larger than ~17 ppm, which is generally accepted as the lower limit for strong H-bonds [27–29]. Despite this large ^{1}H chemical shift, the nitrogens in DMAN*DCPA and DMAN*FDCA are not chemically equivalent, as seen by two resolved ^{15}N chemical shifts (Fig. 2). This is caused by the fact that the bulky organic DCPA and FDCA anions are positioned asymmetrically with respect to the $DMANH^{+}$ cation, creating different chemical environments for the two nitrogens. In comparison, smaller counter anions, such as mineral acids, perchlorate, and tetrafluoroborate, do not exert as large an effect on the ^{15}N chemical environment, as seen from X-ray and ^{15}N NMR studies of Limbach and coworkers [41].

The distinct nitrogen environments affect the basicity of the nitrogen lone-pair electron and in turn the proton localization [27]. Both DMAN*DCPA and DMAN*FDCA show a partially localized proton based on the measured R_{NH} distances, and this proton localization correlates with a decrease in the ^{1}H chemical shift (Fig. 6). This correlation is understandable, since a more covalently bonded proton is more shielded by the heteroatom's electrons. Similar correlations between ^{1}H chemical shifts and R_{NH} have been observed for DMAN salts formed from mineral acids and organic acids [43]. The mineral acids caused more equally shared H^{N} protons, and the resulting H^{N} chemical shifts ranged from 20.7 ppm to 18.8 ppm, whereas the organic acids caused more localized protons, and the ^{1}H chemical shifts ranged from 18.6 to 16.9 ppm. The large effects of the counter anion on the charge density profiles of the DMAN cation have been previously observed in DMAN salts such as DMAN*picrate [41] and DMAN*PF_6 [42–43, 55, 59–60], and even minor polarization differences in the nitrogen lone pair have been shown to cause modest to large changes in R_{NH} and $R_{N\text{---}H}$.

While the two R_{NH} distances in DMAN*DCPA and DMAN*FDCA are not equivalent, both distances are much longer than the covalent bond length of 1.1 Å, and both compounds also have relatively short R_{NN} distances. These results indicate that DMAN complexed with DCPA and FDCA contain a strong NHN^{+} H-bond with an asymmetric double-well potential (Scheme 1d). In comparison, the NHN^{+} H-bond in DMAN*$HClO_4$ has a symmetric double-well potential with a low barrier (Scheme 1e), because a single ^{15}N peak and a single $^{1}H^{N}$ peak was observed at both high and low temperatures. Proton motion in this LBHB is instantaneous but over a very small distance, thus making the two R_{NH} distances indistinguishable. That the DMAN*$HClO_4$ potential energy curve still has a barrier, rather

than being barrier-less (Scheme 1f), is manifested by the fact that the ^{15}N and ^{1}H peaks are both broadened at low temperature, while a barrier-less single-well potential should exhibit no temperature-dependent linewidths or chemical shifts.

In conclusion, the proton position along the H-bond and the strength of the H-bond in DMAN compounds are extremely sensitive to the distant effects of the anion. This sensitivity calls into question the likelihood of establishing and preserving strong H-bonds in complex macromolecules such as proteins. While strong and low-barrier H-bonds have been proposed in proteins such as chymotrypsin, ketosteroid isomerases and M2, the necessary distances are rarely measured. Instead, a large downfield ^{1}H chemical shift is often used as proof of strong H-bonds. However, a large ^{1}H chemical shift is not definitive proof of a strong H-bond, since sidechains and charged residues in close proximity to the H-bond of interest can exert significant influences on the ^{1}H chemical shift. For example, the π-bond node of aromatic sidechains and electrostatic interactions between a downfield proton such as in carboxylic acids (around 12–14 ppm) and another group can cause large downfield ^{1}H chemical shifts. On the other hand, small ^{1}H chemical shifts can rule out the existence of strong H-bonds. In other words, large ^{1}H chemical shifts are a necessary but not sufficient condition for strong or low-barrier H-bonds. For a strong H-bond to exist, the donor - acceptor distance must be significantly shorter than the sum of the van der Waals radii while the proton distance to the two heteroatoms must be significantly longer than the covalent bond length. While the heavy-atom distances can be readily measured by crystallography, the N-H or O-H distance cannot, thus NMR spectroscopy is an important tool for identifying strong H-bonds. In a true low-barrier H-bond, the proton in the H-bond should be equidistant between the donor and acceptor; in other words, the pK_a of the donor and acceptor heteroatoms should be matched. Finally, as well documented in the literature, if the protein of interest functions in solution, then water further reduces the likelihood of LBHBs compared to the solid state because water oxygen can compete with the heteroatoms while the water hydrogen can compete for the lone pairs in the LBHB [61]. For example, Yamaguchi recently reported crystallographic evidence for a LBHB between *para*-coumaric acid and Glu46 in the photoactive yellow protein; but in solution a small ^{1}H chemical shift of 15.2 ppm was found for the OHO^{-} proton, and computational modeling further supported a regular H-bond [5, 8–9]. Thus, transient interactions between water and biomolecules substantially decrease the likelihood of LBHBs in solution. These considerations argue against the presence of LBHBs between the proton-selective histidines in the water-filled pore of the influenza M2 channel, in addition to the experimental evidence of imidazole H^{N} chemical shifts near the water frequency and the X-ray crystal structure of a water cluster at the histidine tetrad.

Supplementary Material

Refer to Web version on PubMed Central for supplementary material.

Acknowledgments

This work is supported by NIH grant GM088204 to M.H. The authors thank Dr. Marc Caporini and Dr. Melanie Rosay at Bruker Biospin for making the 400 and 600 MHz NMR spectrometers available for experiments at 95 K.

The authors would also like to thank Keith Fritzsching for insightful discussions on LBHBs and for initial exploratory experiments.

References

1. Cleland WW, Frey PA, Gerlt JA. The Low Barrier Hydrogen Bond in Enzymatic Catalysis. J Biol Chem. 1998; 273:25529–25532. [PubMed: 9748211]
2. Langkilde A, Kristensen SM, Lo Leggio L, Molgaard A, Jensen JH, Houk AR, Poulsen JCN, Kauppinen S, Larsen S. Short Strong Hydrogen Bonds in Proteins: a Case Study of Rhamnogalacturonan Acetylesterase. Acta Crystallogr D Biol Crystallogr. 2008; 64:851–863. [PubMed: 18645234]
3. Polgar L. The Catalytic Triad of Serine Peptidases. Cell Mol Life Sci. 2005; 62:2161–2172. [PubMed: 16003488]
4. Pollack RM. Enzymatic Mechanisms for Catalysis of Enolization: Ketosteroid Isomerase. Bioorg Chem. 2004; 32:341–353. [PubMed: 15381400]
5. Sigala PA, Tsuchida MA, Herschlag D. Hydrogen Bond Dynamics in the Active Site of Photoactive Yellow Protein. Proc Natl Acad Sci USA. 2009; 106:9232–9237. [PubMed: 19470452]
6. Bondar AN, Fischer S, Smith JC. Water Pathways in the Bacteriorhodopsin Proton Pump. J Membrane Biol. 2011; 239:73–84. [PubMed: 21113780]
7. Mak-Jurkauskas ML, Bajaj VS, Hornstein MK, Belenky M, Griffin RG, Herzfeld J. Energy Transformations Early in the Bacteriorhodopsin Photocycle Revealed by DNP-Enhanced Solid-State NMR. Proc Natl Acad Sci USA. 2008; 105:883–888. [PubMed: 18195364]
8. Nadal-Ferret M, Gelabert R, Moreno M, Lluch JM. Are There Really Low-Barrier Hydrogen Bonds in Proteins? The Case of Photoactive Yellow Protein. J Am Chem Soc. 2014; 136:3542–3552. [PubMed: 24548066]
9. Yamaguchi S, Kamikubo H, Kurihara K, Kuroki R, Niimura N, Shimizu N, Yamazaki Y, Kataoka M. Low-Barrier Hydrogen Bond in Photoactive Yellow Protein. Proc Natl Acad Sci USA. 2009; 106:440–444. [PubMed: 19122140]
10. Hu J, Fu R, Nishimura K, Zhang L, Zhou HX, Busath DD, Vijayvergiya V, Cross TA. Histidines, Heart of the Hydrogen Ion Channel from Influenza A Virus: Toward an Understanding of Conductance and Proton Selectivity. Proc Natl Acad Sci USA. 2006; 103:6865–6870. [PubMed: 16632600]
11. Sharma M, Yi MG, Dong H, Qin HJ, Peterson E, Busath DD, Zhou HX, Cross TA. Insight Into the Mechanism of the Influenza A Proton Channel from a Structure in a Lipid Bilayer. Science. 2010; 330:509–512. [PubMed: 20966252]
12. Frey PA, Whitt SA, Tobin JB. A Low-Barrier Hydrogen-Bond in the Catalytic Triad of Serine Proteases. Science. 1994; 264:1927–1930. [PubMed: 7661899]
13. Lin J, Westler WM, Cleland WW, Markley JL, Frey PA. Fractionation Factors and Activation Energies for Exchange of the Low Barrier Hydrogen Bonding Proton in Peptidyl Trifluoromethyl Ketone Complexes of Chymotrypsin. Proc Natl Acad Sci USA. 1998; 95:14664–14668. [PubMed: 9843946]
14. Loh SN, Markley JL. Hydrogen-Bonding in Proteins as Studied by Amide Hydrogen D/H-Fractionation Factors - Application to Staphylococcal Nuclease. Biochemistry. 1994; 33:1029–1036. [PubMed: 8305430]
15. Markley JL, Westler WM. Protonation-State Dependence of Hydrogen Bond Strengths and Exchange Rates in a Serine Protease Catalytic Triad: Bovine Chymotrypsinogen A. Biochemistry. 1996; 35:11092–11097. [PubMed: 8780512]
16. GarciaViloca M, Gelabert R, GonzalezLafont A, Moreno M, Lluch JM. Is an Extremely Low-Field Proton Signal in the NMR Spectrum Conclusive Evidence for a Low-Barrier Hydrogen Bond? J Phys Chem A. 1997; 101:8727–8733.
17. Garcia-Viloca M, Gelabert R, Gonzalez-Lafont A, Moreno M, Lluch JM. Temperature Dependence of Proton NMR Chemical Shift as a Criterion to Identify Low-Barrier Hydrogen Bonds. J Am Chem Soc. 1998; 120:10203–10209.

18. Schutz CN, Warshel A. The Low Barrier Hydrogen Bond (LBHB) Proposal Revisited: The Case of the Asp…His Pair in Serine Proteases. Proteins-Structure Function and Bioinformatics. 2004; 55:711–723.
19. Warshel A, Papazyan A. Energy Considerations Show That Low-Barrier Hydrogen Bonds Do Not Offer a Catalytic Advantage Over Ordinary Hydrogen Bonds. Proc Natl Acad Sci USA. 1996; 93:13665–13670. [PubMed: 8942991]
20. Warshel A, Papazyan A, Kollman PA. On Low-Barrier Hydrogen-Bonds and Enzyme Catalysis. Science. 1995; 269:102–104. [PubMed: 7661987]
21. Emsley J. Very Strong Hydrogen-Bonding. Chemical Society Reviews. 1980; 9:91–124.
22. Malarski Z, Sobczyk L, Grech E. Structure and IR Spectroscopic Behavior of NHN Hydrogen-Bonds. J Mol Struc. 1988; 177:339–349.
23. Benedict H, Shenderovich IG, Malkina OL, Malkin VG, Denisov GS, Golubev NS, Limbach HH. Nuclear Scalar Spin-Spin Couplings and Geometries of Hydrogen Bonds. J Am Chem Soc. 2000; 122:1979–1988.
24. Brown SP, Perez-Torralba M, Sanz D, Claramunt RM, Emsley L. The Direct Detection of a Hydrogen Bond in the Solid State by NMR Through the Observation of a Hydrogen-Bond Mediated N-15-N-15 J Coupling. J Am Chem Soc. 2002; 124:1152–1153. [PubMed: 11841267]
25. Dingley AJ, Masse JE, Peterson RD, Barfield M, Feigon J, Grzesiek S. Internucleotide Scalar Couplings Across Hydrogen Bonds in Watson-Crick and Hoogsteen Base Pairs of a DNA Triplex. J Am Chem Soc. 1999; 121:6019–6027.
26. Pietrzak M, Limbach HH, Perez-Torralba M, Sanz D, Claramunt RM, Elguero J. Scalar Coupling Constants Across the Intramolecular NHN Hydrogen Bond of Symmetrically and Non-Symmetrically Substituted 6-Aminofulvene-1-aldimines. Magn Reson Chem. 2001; 39:S100–S108.
27. Pietrzak M, et al. Symmetrization of Cationic Hydrogen Bridges of Protonated Sponges Induced by Solvent and Counteranion Interactions as Revealed by NMR Spectroscopy. Chemistry. 2010; 16:1679–1690. [PubMed: 20024986]
28. Brycki B, Brzezinski B, Grech E, Malarski Z, Sobczyk L. H-1 and C-13 NMR-Studies of 1,8-Bis(Dimethylamino)Naphthalene Salts in Acetonitrile-D3. Magn Reson Chem. 1991; 29:558–560.
29. Tobin JB, Whitt SA, Cassidy CS, Frey PA. Low-Barrier Hydrogen-Bonding in Molecular-Complexes Analogous to Histidine and Aspartate in the Catalytic Triad of Serine Proteases. Biochemistry. 1995; 34:6919–6924. [PubMed: 7766600]
30. Hong M, DeGrado WF. Structural Basis for Proton Conduction and Inhibition by the Influenza M2 Protein. Protein Sci. 2012; 21:1620–1633. [PubMed: 23001990]
31. Wang C, Lamb RA, Pinto LH. Activation of the M2 Ion Channel of Influenza Virus: A Role for the Transmembrane Domain Histidine Residue. Biophys J. 1995; 69:1363–1371. [PubMed: 8534806]
32. Pinto LH, Dieckmann GR, Gandhi CS, Papworth CG, Braman J, Shaughnessy MA, Lear JD, Lamb RA, DeGrado WF. A Functionally Defined Model for the M2 Proton Channel of Influenza A Virus Suggests a Mechanism for Its Ion Selectivity. Proc Natl Acad Sci USA. 1997; 94:11301–11306. [PubMed: 9326604]
33. Hu F, Luo W, Hong M. Mechanisms of Proton Conduction and Gating by Influenza M2 Proton Channels from Solid-State NMR. Science. 2010; 330:505–508. [PubMed: 20966251]
34. Hu FH, Schmidt-Rohr K, Hong M. NMR Detection of pH-Dependent Histidine-Water Proton Exchange Reveals the Conduction Mechanism of a Transmembrane Proton Channel. J Am Chem Soc. 2012; 134:3703–3713. [PubMed: 21974716]
35. Acharya A, et al. Structural Mechanism of Proton Transport Through the Influenza A M2 Protein. Proc Natl Acad Sci U S A. 2010; 107:15075–15080. [PubMed: 20689043]
36. Hong M, Fritzsching KJ, Williams JK. Hydrogen-Bonding Partner of the Proton-Conducting Histidine in the Influenza M2 Proton Channel Revealed From H-1 Chemical Shifts. J Am Chem Soc. 2012; 134:14753–14755. [PubMed: 22931093]
37. Andreas LB, Eddy MT, Pielak RM, Chou JJ, Griffin RG. Magic Angle Spinning NMR Investigation of Influenza A M2(18-60): Support for an Allosteric Mechanism of Inhibition. J Am Chem Soc. 2010; 132:10958–10960. [PubMed: 20698642]

38. Andreas LB, Eddy MT, Chou JJ, Griffin RG. Magic-Angle-Spinning NMR of the Drug Resistant S31N M2 Proton Transporter From Influenza A. J Am Chem Soc. 2012; 134:7215–7218. [PubMed: 22480220]
39. Colvin MT, Andreas LB, Chou JJ, Griffin RG. Proton Association Constants of His 37 in the Influenza-A M218-60 Dimer-of-Dimers. Biochemistry. 2014; 53:5987–5994. [PubMed: 25184631]
40. Glowiak T, Malarski Z, Sobczyk L, Grech E. New Example of a Symmetrical Nhn Hydrogen-Bond in Protonated 1,8-Bis(Dimethylamino)Naphthalene (DMAN). J Mol Struc. 1992; 270:441–447.
41. Lopez C, Claramunt RM, LlamasSaiz AL, FocesFoces C, Elguero J, Sobrados I, AguilarParrilla F, Limbach HH. X-Ray Diffraction and Solid State NMR Studies of 1,8-Bis(dimethylamino)naphthalene and Its Complexes with Picric and Hexafluorophosphoric Acids. New J Chemistry. 1996; 20:523–536.
42. Parkin A, Wozniak K, Wilson CC. From Proton Disorder to Proton Migration: A Continuum in the Hydrogen Bond of a Proton Sponge in the Solid State. Crystal Growth & Design. 2007; 7:1393–1398.
43. Wozniak K, He HY, Klinowski J, Barr TL, Milart P. ESCA and Solid-State NMR Studies of Ionic Complexes of 1,8-Bis(dimethylamino)naphthalene. J Phys Chem. 1996; 100:11420–11426.
44. Crivello JV. Nitrations and Oxidations with Inorganic Nitrate Salts in Trifluoroacetic-Anhydride. J Org Chem. 1981; 46:3056–3060.
45. Kurasov LA, Pozharskii AF, Kuzmenko VV. Peri-Naphthylenediamines .3. Convenient Method for the Alkylation of 1,8-Naphthylenediamines and Perimidines. Zhurnal Organicheskoi Khimii. 1981; 17:1944–1947.
46. Lloyd-Jones GC, Harvey JN, Hodgson P, Murray M, Woodward RL. Scalar Coupling Between the N-15 Centres in Methylated 1,8-Diaminonaphthalenes and 1,6-Diazacyclodecane: To What Extent is (2H)J(NN) a Reliable Indicator of N-N Distance? Chemistry-a European Journal. 2003; 9:4523–4535.
47. Ni WH, Dongsheng, Shi Feng, Xue Dongjie, Yang Haizhou. Hydrazine-Hydrate Catalyzed Preparation of 1,8-Dimethylaminonapthalene from 1,8-Dinitronaphthalene. 2010 CN 101823968A.
48. Li S, Su Y, Luo W, Hong M. Water-protein Interactions of an Arginine-Rich Membrane Peptide in Lipid Bilayers Investigated by Solid-State Nuclear Magnetic Resonance Spectroscopy. J Phys Chem B. 2010; 114:4063–4069. [PubMed: 20199036]
49. Hong M, Gross JD, Rienstra CM, Griffin RG, Kumashiro KK, Schmidt-Rohr K. Coupling Amplification in 2D MAS NMR and Its Application to Torsion Angle Determination in Peptides. J Magn Reson. 1997; 129:85–92. [PubMed: 9405219]
50. Bielecki A, Kolbert AC, Levitt MH. Frequency-Switched Pulse Sequences: Homonuclear Decoupling and Dilute Spin NMR in Solids. Chem Phys Lett. 1989; 155:341–346.
51. Hong M, Griffin RG. Resonance Assignment for Solid Peptides by Dipolar-Mediated 13C/15N Correlation Solid-State NMR. J Am Chem Soc. 1998; 120:7113–7114.
52. Rienstra CM, Hohwy M, Hong M, Griffin RG. 2D and 3D 15N-13C-13C NMR Chemical Shift Correlation Spectroscopy of Solids: Assignment of MAS Spectra of Peptides. J Am Chem Soc. 2000; 122:10979–10990.
53. van Rossum BJ, de Groot CP, Ladizhansky V, Vega S, de Groot HJM. A Method for Measuring Heteronuclear (H-1-C-13) Distances in High Speed MAS NMR. J Am Chem Soc. 2000; 122:3465–3472.
54. Hong M, Yao XL, Jakes K, Huster D. Investigation of Molecular Motions by Lee-Goldburg Cross-Polarization NMR Spectroscopy. J Phys Chem B. 2002; 106:7355–7364.
55. Hoser AA, Dobrzycki L, Gutmann MJ, Wozniak K. Charge Densities of Two Polymorphs of Hydrated 1,8-Bis(dimethylamino)naphthalene Hydrochloride-Similarities and Differences. Crystal Growth & Design. 2010; 10:5092–5104.
56. Pyzalska D, Pyzalski R, Borowiak T. Structure of 1,8-Bis(Dimethylamino)Naphthalene Hydrobromide Dihydrate. J Cryst Spectros Res. 1983; 13:211–220.

57. Wozniak K, Krygowski TM, Kariuki B, Jones W, Grech E. Crystallographic Studies on Sterically Affected Chemical-Species .2. Molecular and Crystal-Structure of 1,8-Bis(Dimethylamino)-Naphthalene Tetrafluoroborate - Analysis of Distortion of Geometry in the Aromatic Part Due to Intramolecular Hydrogen-Bonding. J Mol Struc. 1990; 240:111–118.

58. Song XJ, McDermott AE. Proton Transfer Dynamics and N-H Bond Lengthening in N-H Center dot Center dot Center dot N Model Systems: a Solid-State NMR Study. Magn Reson Chem. 2001; 39:S37–S43.

59. Lopez C, Lorente P, Claramunt RM, Marin J, Foces-Foces C, Llamas-Saiz AL, Elguero J, Limbach HH. Localization of Hydrogen Bond Deuterons in Proton Sponges by Dipolar Solid State N-15 NMR Spectroscopy. Berichte Der Bunsen-Gesellschaft-Physical Chemistry Chemical Physics. 1998; 102:414–418.

60. Mallinson PR, Smith GT, Wilson CC, Grech E, Wozniak K. From Weak Interactions to Covalent Bonds: A Continuum in the Complexes of 1,8-Bis(dimethylamino)naphthalene. J Am Chem Soc. 2003; 125:4259–4270. [PubMed: 12670248]

61. Frey PA, Cleland WW. Are There Strong Hydrogen Bonds in Aqueous Solutions? Bioorganic Chemistry. 1998; 26:175–192.

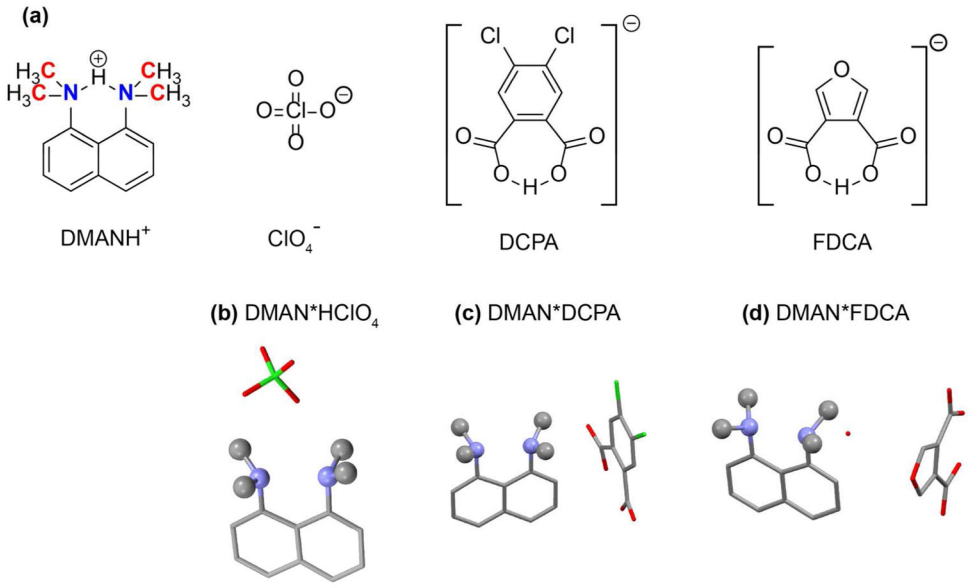

Figure 1.

Structures of the DMAN salts used in this study. (a) Chemical structures. (b–d) X-ray crystal structures. (b) DMAN*$HClO_4$. (c) DMAN*DCPA. (d) DMAN*FDCA. Hydrogen atoms are omitted for clarity. The structure for DMAN*DCPA is reproduced from reference [42].

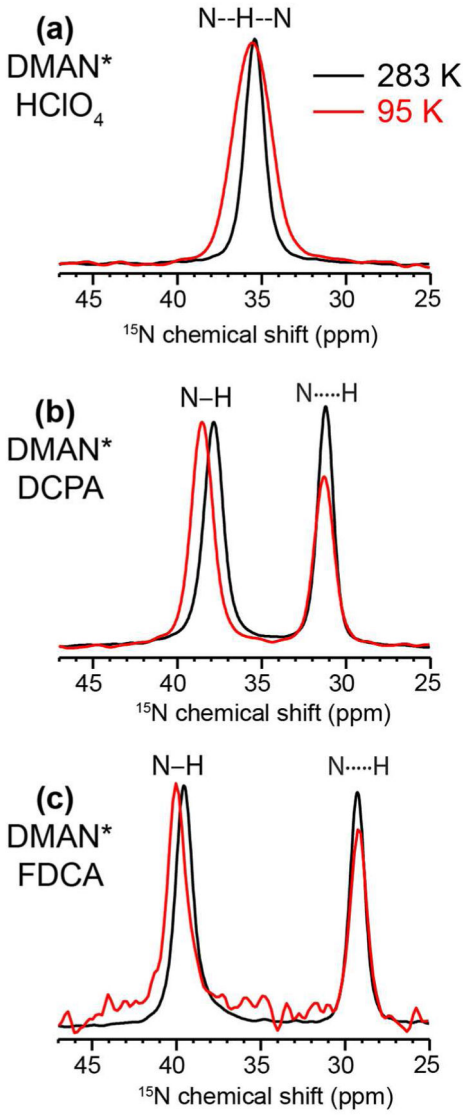

Figure 2.

^{15}N CPMAS spectra of DMAN salts at 283 K and 95 K. (a) DMAN*$HClO_4$. (b) DMAN*DCPA. (c) DMAN*FDCA. The N-H and N···H assignment is based on the DIPSHIFT data in Fig. 3.

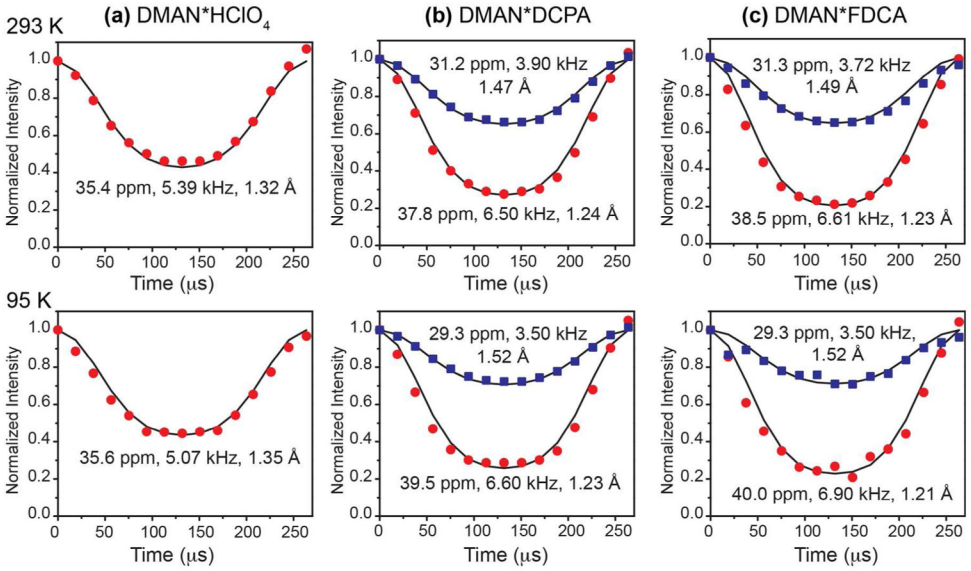

Figure 3.

^{15}N-^{1}H doubled-DIPSHIFT data of DMAN salts at 293 K (top) and 95 K (bottom). (a) DMAN*$HClO_4$. (b) DMAN*DCPA. (c) DMAN*FDCA. The data were obtained under 3.79 kHz MAS. Solid lines are best-fit simulations. The listed N-H dipolar coupling strengths are true values after taking into account the experimental FSLG scaling factor and the doubling factor. The ^{15}N chemical shift and the N-H distances are also indicated.

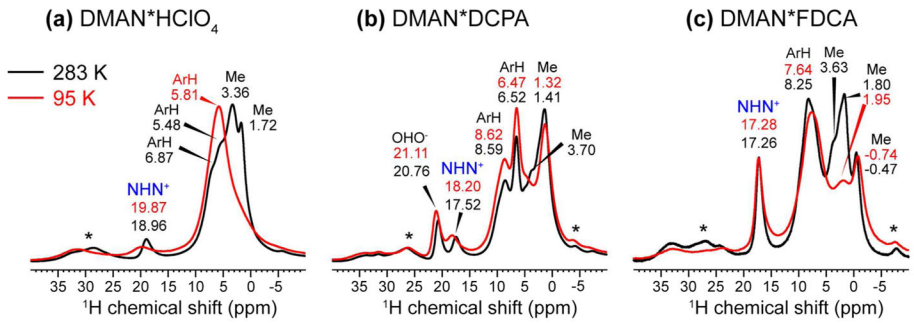

Figure 4.

^{1}H MAS spectra of DMAN salts at 283 K (black) and 95 K (red) under 15 kHz MAS. Assignment is based on the general chemical shift trends of aromatic, H^{N}, and aliphatic protons. Asterisks indicate spinning sidebands.

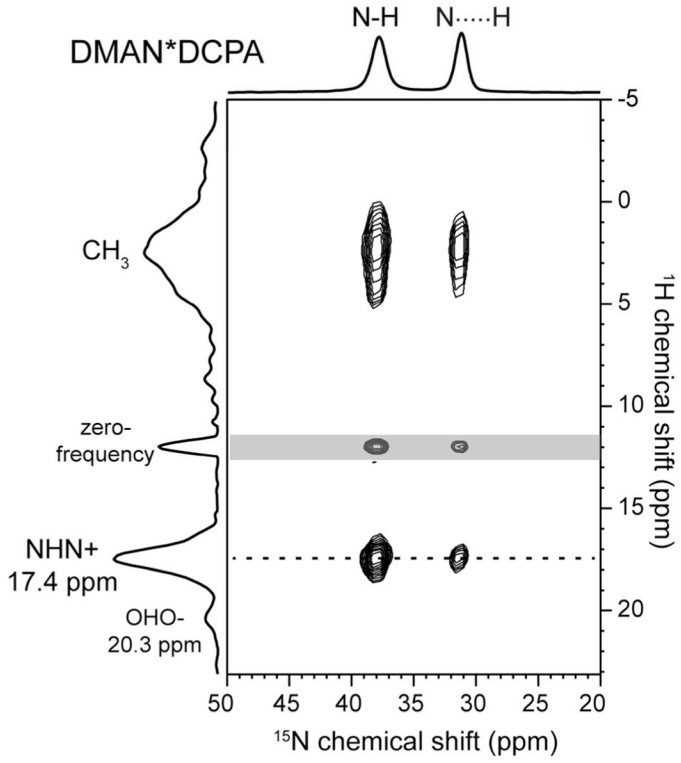

Figure 5.

2D ^{15}N-^{1}H HETCOR spectrum of DMAN*DCPA at 293 K under 7.58 kHz MAS. The ^{1}H chemical shift is the true value after taking into account the FLSG scaling factor of 0.577.

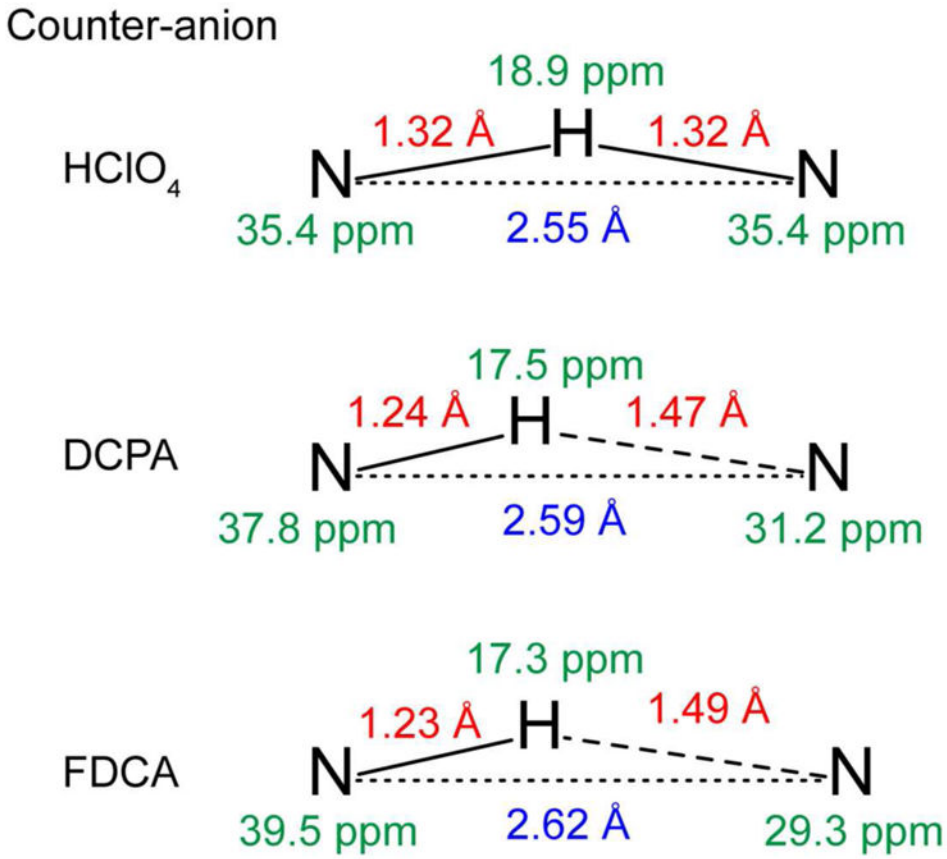

Figure 6.

Summary of the ^{1}H and ^{15}N NMR chemical shifts (green), N-H bond lengths (red), and crystallographically determined N---N distances (blue) of the three DMAN salts. DMAN*$HClO_4$ shows the most delocalized H^N or the strongest H-bond, the largest ^{1}H chemical shift and equivalent ^{15}N chemical shifts. The two DMAN salts with bulky organic counter anions have different R_{NH}'s, inequivalent ^{15}N chemical shifts, and smaller ^{1}H chemical shifts.

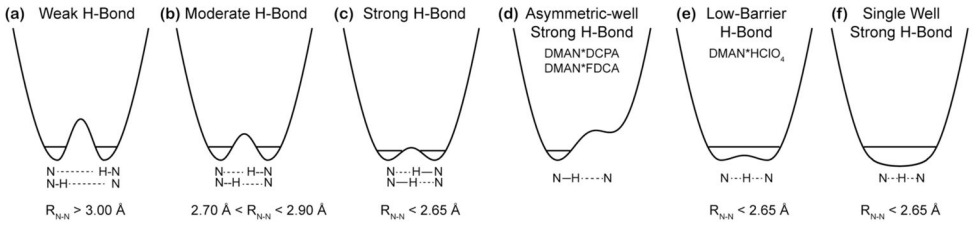

Scheme 1.

Physical and energetic properties of NHN hydrogen bonds and proposed potentialenergy wells for the DMAN*HX salts studied here.

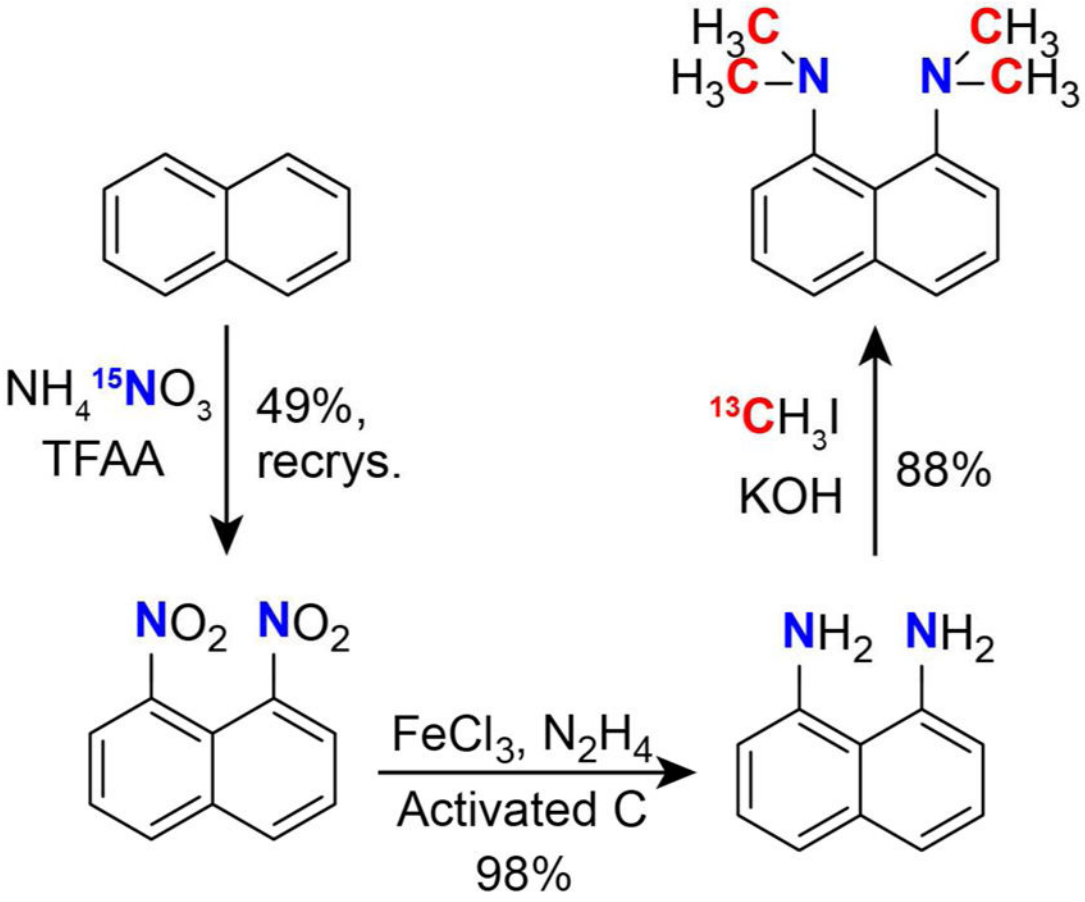

Scheme 2.
Synthetic route to DMAN.

Table 1

Unit cell parameters of the crystal structures of the three DMAN salts used in this study.

	DMAN*HClO4	DMAN*DCPA	DMAN*FDCA
Crystal Group	**Fdd2**	**P1**	**P21/n**
α (°)	90.00	75.13	90.00
β (°)	90.00	71.23	91.65
γ (°)	90.00	70.62	90.00
a (Å)	12.55	9.30	11.24
b (Å)	46.88	9.63	10.28
c (Å)	10.24	13.03	16.69
Volume ($Å^3$)	6022.69	1027.63	1928.04